Neuron
Article

A Central Role for the ERK-Signaling Pathway in Controlling Schwann Cell Plasticity and Peripheral Nerve Regeneration In Vivo

Ilaria Napoli,[1,3] Luke A. Noon,[1,3] Sara Ribeiro,[1] Ajay P. Kerai,[1] Simona Parrinello,[1] Laura H. Rosenberg,[1] Melissa J. Collins,[1] Marie C. Harrisingh,[1] Ian J. White,[1] Ashwin Woodhoo,[2] and Alison C. Lloyd[1,*]
[1]MRC Laboratory for Molecular Cell Biology and the UCL Cancer Institute, University College London, Gower Street, London WC1E 6BT, UK
[2]Department of Cell and Developmental Biology, University College London, Gower Street, London WC1E 6BT, UK
[3]These authors contributed equally to this work
*Correspondence: alison.lloyd@ucl.ac.uk
DOI 10.1016/j.neuron.2011.11.031

SUMMARY

Following damage to peripheral nerves, a remarkable process of clearance and regeneration takes place. Axons downstream of the injury degenerate, while the nerve is remodeled to direct axonal regrowth. Schwann cells are important for this regenerative process. "Sensing" damaged axons, they dedifferentiate to a progenitor-like state, in which they aid nerve regeneration. Here, we demonstrate that activation of an inducible Raf-kinase transgene in myelinated Schwann cells is sufficient to control this plasticity by inducing severe demyelination in the absence of axonal damage, with the period of demyelination/ataxia determined by the duration of Raf activation. Remarkably, activation of Raf-kinase also induces much of the inflammatory response important for nerve repair, including breakdown of the blood-nerve barrier and the influx of inflammatory cells. This reversible in vivo model identifies a central role for ERK signaling in Schwann cells in orchestrating nerve repair and is a powerful system for studying peripheral neuropathies and cancer.

INTRODUCTION

Peripheral nerves are complex structures consisting of motor, sensory and autonomic neurons, which connect tissues and organs to the central nervous system (CNS). Within the nerves, the axons of individual neurons are intimately associated with the major glia of the peripheral nervous system (PNS), Schwann cells. Larger axons associate in a 1:1 fashion with myelinating Schwann cells, whereas nonmyelinating Schwann cells bundle smaller axons together in structures known as Remak bundles. Groups of Schwann cell-enwrapped axons are further bundled into structures known as fascicles by perineural fibroblasts, and large nerves consist of several of these fascicles wrapped by the epineurium. Like the CNS, the PNS is a privileged environment, with specialized blood vessels within the nerve maintaining a blood-nerve barrier (BNB) (Choi and Kim, 2008). Despite their complex structure, peripheral nerves are one of the few mammalian tissues with the capacity for extensive regeneration. Following a nerve injury, axons downstream of the damage degenerate in an active process known as Wallerian degeneration. The associated Schwann cells dedifferentiate to a progenitor-like state and proliferate and, together with infiltrating macrophages, clear the axonal and myelin debris. This period is associated with a robust inflammatory response: the BNB is breached and inflammatory cells enter the nerve in large numbers—both at the damage site and throughout the length of the distal stump. The axons regrow from upstream of the site of damage using "tubes" of progenitor-like Schwann cells, which remain within their basal lamina, to guide them back to their original target tissues. The Schwann cells then redifferentiate to fully restore nerve function and the inflammatory response resolves (Stoll et al., 2002; Zochodne, 2008).

Several pathologies have been linked to aberrations in this repair process. Neurofibromas, the major tumor type of this tissue, are most frequently seen in patients with the common genetic disorder neurofibromatosis type 1 (NF1). These tumors are often referred to as "unrepaired wounds," as they consist of a mixture of progenitor-like Schwann cells, dissociated from axons, infiltrated by large numbers of inflammatory cells, which have been reported to have an important role in tumor development (Parrinello and Lloyd, 2009). Similarly, many peripheral neuropathies are associated with demyelination and frequently an inflammatory response (Stoll et al., 2002; Suter and Scherer, 2003). However, despite the importance of understanding the regenerative nature of this tissue and important implications for disease, the molecular nature of the response, and how the complex cellular processes are coordinated remain poorly understood.

We have previously shown that activation of the Raf/MEK/ERK signaling pathway is sufficient to induce dedifferentiation of myelinated Schwann cells in vitro (Harrisingh et al., 2004). Moreover, we and others have shown that there is a rapid and robust activation of ERK signaling in Schwann cells following nerve injury, both at the injury site and throughout the distal stump (Harrisingh et al., 2004; Sheu et al., 2000). Interestingly, high levels of ERK activity have also been observed in Schwann cells in models of both inherited and infectious peripheral

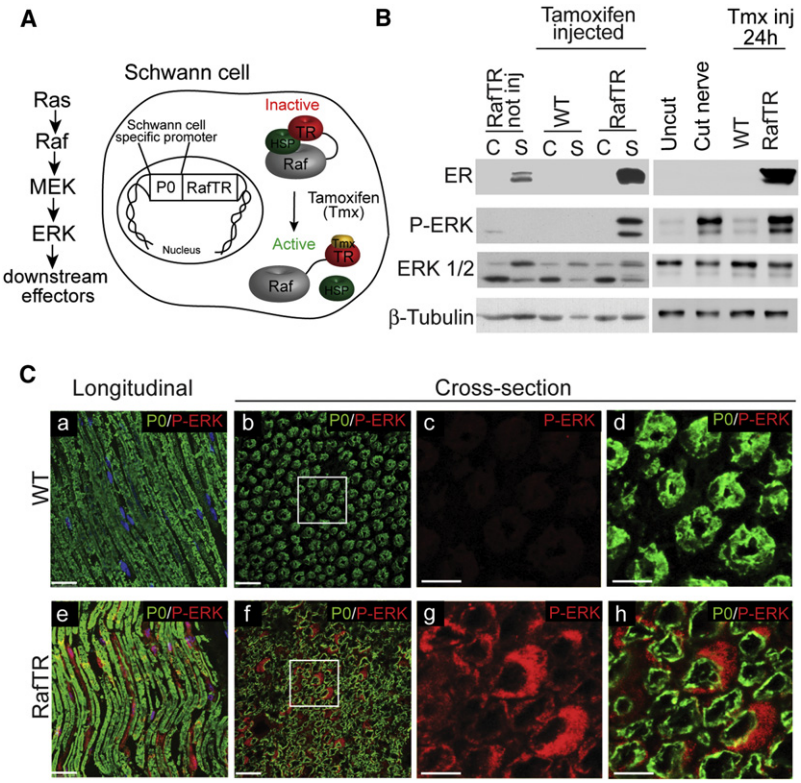

Figure 1. The Raf/ERK Pathway Is Specifically Activated in Schwann Cells in P0-RafTR Transgenic Mice

(A) Schematic illustrations of the Ras/Raf/MEK/ERK pathway and of a Schwann cell in the P0-RafTR transgenic mice. The Raf kinase/estrogen receptor fusion protein is expressed under the control of the Schwann cell specific P0 promoter in an inactive state. In the presence of tamoxifen, RafTR is activated and stimulates the ERK signaling pathway.

(B) Western blot analysis of RafTR protein expression (ER) and ERK activation (P-ERK) following tamoxifen injection. Left panel: protein lysates from CNS (cerebral cortex-C) and PNS (sciatic nerve-S) of WT and P0-RafTR mice, noninjected or 24 hr post-tamoxifen injection. Right panel: "uncut" and "cut" nerve extracts from WT sciatic nerves 24 hr postsurgery and P0-RafTR and WT sciatic nerve lysates, 24 hr post-Tmx injection.

(C) Confocal images of longitudinal or cross-sections of sciatic nerve immunostained for P-ERK (red) and the myelin protein P0 (green) in WT (a–d) and P0-RafTR (e–h) tamoxifen-injected mice; (c and d) and (g and h) show zoomed regions of (b) and (f). Scale bar is 25 μm (a, b, e, and f) and 10 μm (c, d, g, and h).

See also Figure S1.

neuropathies (Fischer et al., 2008; Nadra et al., 2008; Tapinos et al., 2006). Moreover, ERK activation occurs in Schwann cell tumors that arise in NF1, as a result of excessive Ras signaling secondary to the loss of the Ras-GAP neurofibromin that is encoded by *NF1* (McClatchey, 2007). However, recent mouse models of NF1 have indicated that neurofibromin loss is unable to drive Schwann cell dedifferentiation in the adult nerve (Joseph et al., 2008; Wu et al., 2008; Zheng et al., 2008), and other signaling pathways have been linked to the dedifferentiation process (Jessen and Mirsky, 2008; Parkinson et al., 2008; Woodhoo et al., 2009), leading to speculation that a single signaling pathway may be insufficient to drive the dedifferentiation process in the context of a fully functional adult nerve.

To address these issues we constructed a transgenic mouse which, by targeting a tamoxifen (Tmx)-inducible Raf-kinase/estrogen receptor fusion protein (RafTR) specifically to myelinating Schwann cells, enabled us to rapidly and reversibly activate the Raf/MEK/ERK signaling pathway in adult myelinating Schwann cells—permitting a temporal analysis of the effects of activating Raf/MEK/ERK signaling in Schwann cells in vivo. We found that activation of Raf-kinase was sufficient to drive the dedifferentiation of myelinating Schwann cells to a progenitor-like state in peripheral adult nerves, resulting in severe loss of motor function. Importantly, the demyelinated phenotype was independent of axonal degradation—the normal injury signal—but was instead determined by the period of ERK activation, with rapid remyelination and neurological recovery taking place following the withdrawal of tamoxifen. Interestingly, despite the absence of injury, Raf activation in Schwann cells resulted in the breakdown of the BNB and the recruitment of inflammatory cells, a response mimicked by the activation of Raf/MEK/ERK signaling in Schwann cells in vitro. Our results identify the Schwann cell as a central organizer of the complex cellular response required for peripheral nerve repair and the Raf/MEK/ERK signaling pathway as the key intracellular mediator of these responses.

RESULTS

To address the role of the Raf/MEK/ERK signaling pathway in vivo, we developed an inducible transgenic mouse-model system that allowed us to regulate ERK signaling in myelinating Schwann cells in the adult. To do this, we expressed a tamoxifen (Tmx)—inducible Raf-kinase/estrogen receptor fusion protein (RafTR) (Samuels et al., 1993) under the control of a myelinating Schwann cell-specific promoter (Figure 1A). The expression of this fusion protein allows the rapid and reversible activation of Raf kinase activity and the downstream MEK/ERK kinase cascade following the addition of hormone (Figure 1A). To ensure robust expression, we used a modified rat myelin protein zero (P0) promoter containing intronic and non-translated 3′ and 5′ elements of the human connexin-32 gene, which has previously been shown to enhance expression in myelinated Schwann cells (Figure 1A and see Figure S1 available online; Huang et al., 2005; Scherer et al., 2005). This construct should direct the expression of inactive RafTR protein in these cells throughout the PNS. The RafTR fusion protein contains a point mutation in the human estrogen receptor ligand-binding domain, so that it can be activated by the injection of the estrogen analog tamoxifen but not by endogenous estrogens. Following pronuclear injection of the linearized construct, we obtained 8 RafTR-positive mice,

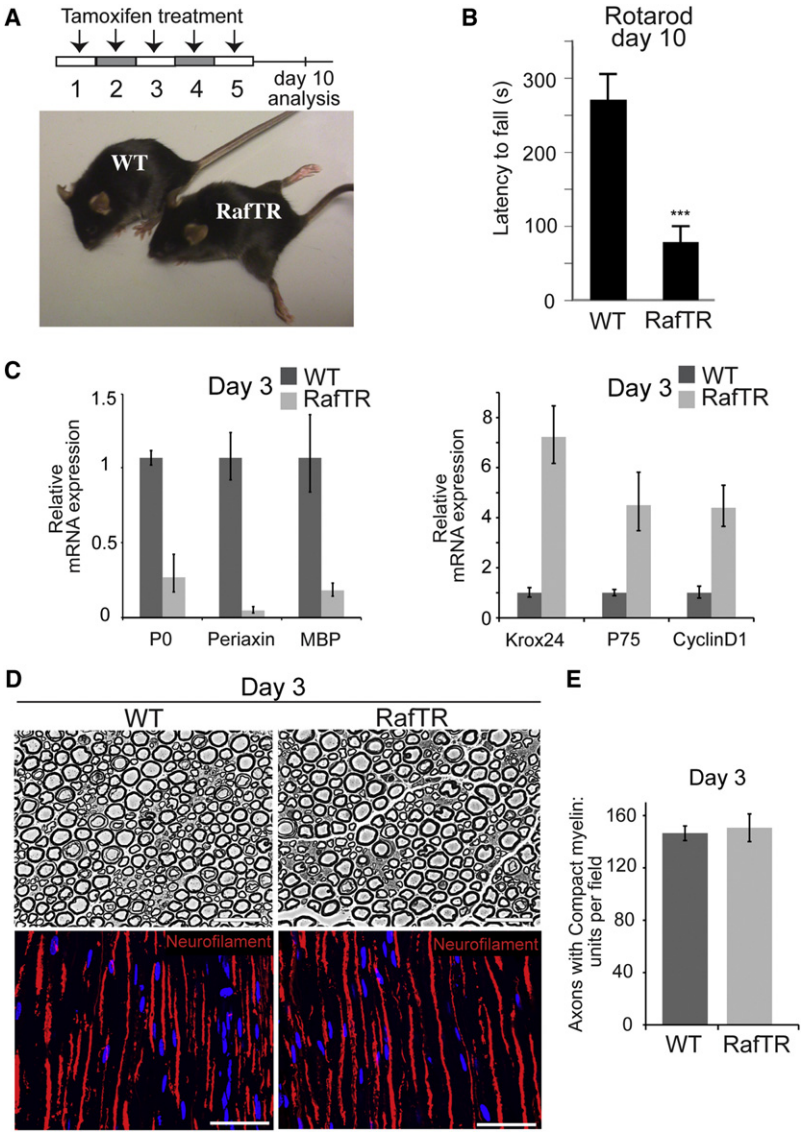

Figure 2. Raf Activation in Schwann Cells Causes a Severe Loss of Motor Function; Myelin Gene Expression Is Downregulated

(A) Schematic illustration of the protocol used for tamoxifen injections. P0-RafTR but not WT mice exhibit severe motor function defects by day 10, with abnormal hind-limb posture following tamoxifen injections.

(B) WT and P0-RafTR adult mice were tested using an accelerating rotarod for a maximum of 300 s on day 10. Mean latency to fall (in seconds, ± SEM) is plotted (n = 10 animals for each group). See also Movies S1 and S2.

(C) qRT-PCR analysis of RNA from sciatic nerves of WT and P0-RafTR mice, after 72 hr of daily tamoxifen injections. The bar graphs represent the relative transcript levels of indicated genes (n = 4 animals for each group, data are represented as mean values ± SEM).

(D) Representative phase-microscopy images of semi-thin cross-sections of sciatic nerves from WT and P0-RafTR mice stained with toluidine blue after 72 hr of daily tamoxifen injections (top panels). Scale bar is 20 μm. Longitudinal sections of sciatic nerves stained for neurofilament (red) and nuclei stained with Hoechst (blue). Scale bar is 50 μm (bottom panels).

(E) Quantification of myelinated fibers in WT and P0-RafTR mice at day 3 (n = 3 animals for each group, 3 different fields were counted for each animal, data are represented as mean values ± SEM).

See also Figure S2.

two of which produced lines with detectable expression of RafTR mRNA and protein in sciatic nerve. The RafTR-expressing mice were crossed with wild-type (WT) animals, and in all subsequent experiments heterozygous P0-RafTR mice were compared with their WT, age-matched littermates. Similar results were obtained with both P0-RafTR lines.

To confirm the specificity of expression of the construct and the inducibility of the Raf-kinase activity, we initially gave the mice a single intraperitoneal (IP) injection of tamoxifen and analyzed the mice after 24 hr. As controls, we compared the injected P0-RafTR mice to both uninjected P0-RafTR mice and to tamoxifen-injected WT controls. Western blot analysis detected the RafTR protein in peripheral nerve extracts from P0-RafTR mice but not in WT controls (Figure 1B). Moreover, the fusion protein could not be detected in cortical brain extracts, confirming the specificity of expression. Levels of RafTR protein were higher in the injected animals compared to uninjected RafTR-expressing controls, which is consistent with the reported stabilization of the protein upon tamoxifen binding. Importantly, Raf-kinase activity, as measured by the level of the phosphorylated downstream effector ERK (P-ERK), was induced in the PNS but not the CNS following tamoxifen injection (Figure 1B). Increased levels of P-ERK were not detectable in either WT animals injected with tamoxifen or uninjected P0-RafTR animals, confirming the tight regulation of the Raf kinase in the mouse. Immunolabeling of sciatic nerves demonstrated that ERK was activated specifically in myelinated Schwann cells following tamoxifen injection, confirming the inducible nature of the kinase in the intended target cells (Figure 1C). The magnitude of P-ERK induction was similar to that seen in the distal stump of cut WT sciatic nerves 24 hr following nerve transection, indicating that we are activating the ERK pathway in P0-RafTR nerves to levels similar to those seen following an injury response in WT nerves (Figures 1B, 1C, and S1B).

Following injury, high levels of P-ERK are rapidly induced in myelinating Schwann cells and persist for 3–5 days (Harrisingh et al., 2004). To mimic this, control and transgenic mice (aged 4–6 weeks) were given 5 consecutive daily IP tamoxifen injections and their behavior was monitored daily. In control animals, the injections had no observable effect. In contrast, at day 7–8 we noticed the animals were weaker and by day 10, the P0-RafTR mice displayed severe impairment of coordination and positioning of their limbs, consistent with a demyelinating phenotype (Figure 2A). In some cases, the effects were so severe

that the mice were unable to support their own body weight (Movie S1). Hind-paw prints from injected P0-RafTR mice were more elongated and had reduced "toespread" compared to injected WT littermates (Figure S2)—signs indicative of peripheral nerve damage (Crawley, 2008). Furthermore, a large impairment in motor coordination was observed as measured by the accelerating rotarod test (Movie S2); and quantified in Figure 2B. These results show that Raf-kinase activation in myelinated Schwann cells is sufficient to drive a rapid loss of peripheral nerve function in vivo, consistent with nerve demyelination.

Our previous in vitro studies have shown that Raf/MEK/ERK driven Schwann cell dedifferentiation is associated with the downregulation of myelin-specific gene expression and the upregulation of genes expressed by dedifferentiated Schwann cells (Harrisingh et al., 2004). Quantitative RT-PCR analysis of nerves isolated from tamoxifen-injected P0-RafTR animals showed that by day 3 following the first injection (day 3) the expression of myelin genes were strongly downregulated. (Figure 2C). Conversely, markers of dedifferentiated Schwann cells in the adult, *Krox-24* and *p75* (also expressed by nonmyelinating Schwann cells), together with the proliferation marker *cyclin D1*, were strongly upregulated (Figure 2C). However, analysis of sciatic nerves from these mice showed that at day 3, the structure of the nerves was indistinguishable from that of WT injected animals, with no differences in the degree of myelination (Figures 2D and 2E), demonstrating that changes in gene expression occurred prior to myelin breakdown. Moreover, axonal staining showed that the axons remained intact (Figure 2D).

The downregulation of myelin gene expression observed on day 3 was sustained in the nerves of transgenic mice on day 10, when the motor dysfunction was severe (Figure 3A). However, when the structure of peripheral nerves was analyzed at this time, a dramatic change in histology was observed: most notably, there was widespread breakdown of myelin and increased cellularity in the intraneural spaces (Figures 3B and 3C). Quantification of the extent of demyelination confirmed a large decrease in the number of Schwann cell/axon units containing compact myelin (Figure 3D) and many of the remaining units displayed myelin infoldings and outfoldings together with vacuoles of degraded myelin protein, which are characteristic of demyelination in injured nerves. Immunostaining of the nerve showed a large increase in the number of p75-positive cells, confirming that these cells had dedifferentiated back to a progenitor-like state (Figure 3B). Interestingly, despite the breakdown of the myelin sheaths and the dedifferentiation of the Schwann cells, the axons remained intact, as determined by EM, neurofilament staining and that the levels of neuronal-specific *tau* mRNA levels remained unchanged (Figures 3A, 3B, and S3A–S3C). In contrast, at similar time points following nerve damage, only minor fragments of axonal debris remained within the nerve and neurofilament protein was no longer detectable (Figure S3B). Although the degree of demyelination was severe in the P0-RafTR mice, it was not complete, as some axons were still myelinated. To determine whether the incomplete phenotype was due to insufficient levels of tamoxifen throughout the nerve, we performed intraneural injections of tamoxifen into several P0-RafTR and control mice (Figure S3D). Consistent with this hypothesis, we found complete demyelination of nerves in the proximity of the injection site. Importantly, this occurred in the absence of observable axonal damage and the structure of the nerve was normal in sections far from the injection site (Figures S3E and S3F). Thus, activation of Raf-kinase activity in myelinating Schwann cells is sufficient to drive Schwann cell dedifferentiation in adult nerve without causing axonal damage.

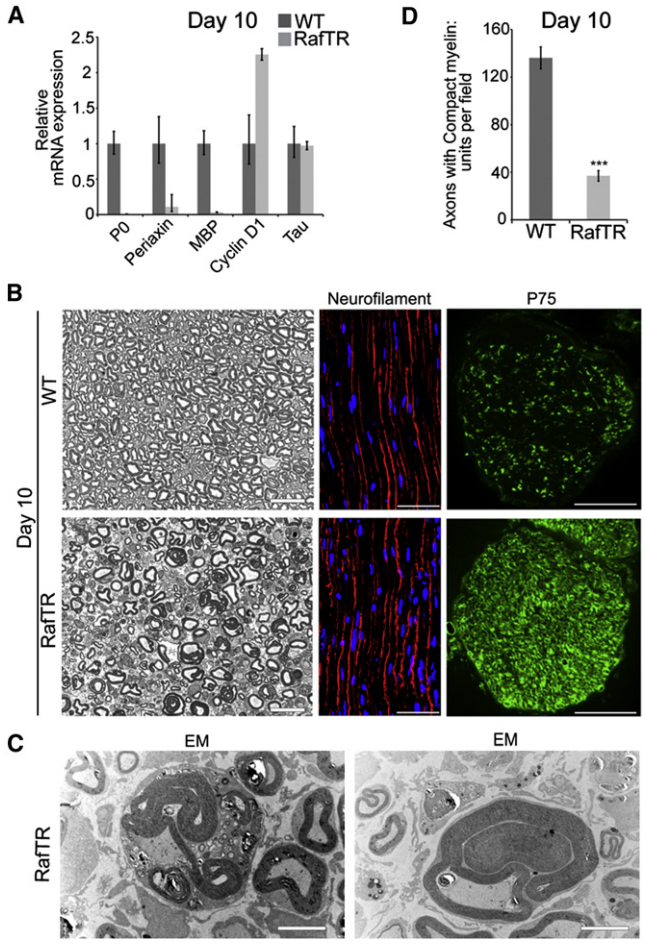

Figure 3. Raf Activation in Schwann Cells Drives PNS Demyelination in the Absence of Axonal Injury

(A) qRT-PCR analysis of RNA from sciatic nerves of WT and P0-RafTR mice 10 days after the first tamoxifen injection (day 10) when transgenic mice exhibit severe motor dysfunction. The bar graphs represent the relative transcript levels of indicated genes ± SEM (n = 4 for each group).

(B) Representative images of sciatic nerve sections from WT and P0-RafTR mice on day 10. Left panel: phase-contrast images of toluidine blue stained, semi-thin cross-sections. Scale bar is 20 μm. Middle panels: longitudinal sections immunolabeled for neurofilament (red) and nuclei stained with Hoechst (blue). Scale bar 50 μm. Right panels: cross-sections immunolabeled for p75 (green); scale bar 250 μm. Four animals were examined for each condition and all animals showed a similar phenotype.

(C) Electron micrographs showing examples of demyelination in P0-RafTR mice sciatic nerve. Scale bar 5 μm.

(D) Quantification of myelinated fibers in WT and P0-RafTR mice at day 10 (n = 4 animals for each group, 3 different fields were counted for each animal and data are represented as mean values ± SEM).

See also Figure S3.

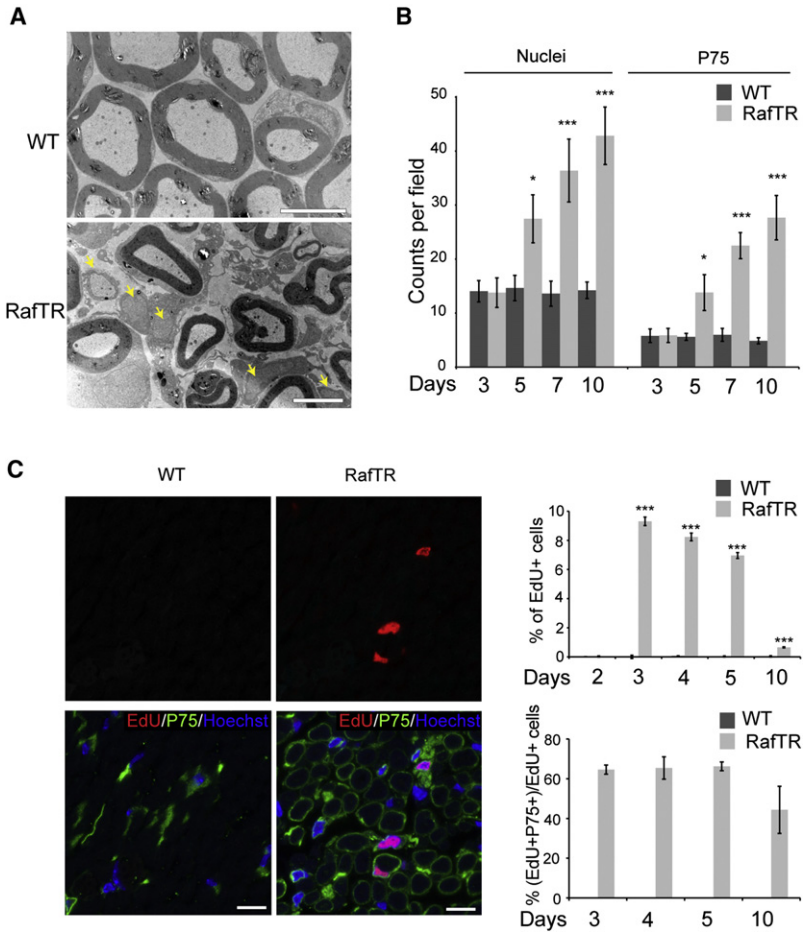

Figure 4. Increased Schwann Cell Proliferation in Demyelinated P0-RafTR Nerves

(A) Electron micrographs of cross-sections of WT and P0-RafTR mice at day 10. Note the increased number of cells (yellow arrows) and collagen deposition. Scale bar is 5 μm.

(B) Cryosections of WT and P0-RafTR mice at indicated time-points following tamoxifen treatment were stained with Hoechst and P75 antibody to label Schwann cells. Graphs show quantification of nuclei (LHS) and p75-positive cells (RHS) per field of view at the indicated time points (n = 4 animals for each group at each time point, 8 different fields were counted for each animal, data are represented as mean values ± SEM).

(C) WT and P0-RafTR mice were injected with EdU, 4 hr prior to sacrifice. Left panel: representative images of EdU labeling (red) of WT and P0-RafTR mice costained for p75 (green) at day 5. Scale bar 10 μm. Right panel: quantification of the percentage of EdU positive cells (upper graph) and the percentage of EdU-positive cells that are P75 positive (proliferating Schwann cells) (lower graph) in WT and RafTR sciatic nerves at indicated time points (n = 3 animals for each group at each time point, 8 different fields were counted for each animal, data are represented as mean values ± SEM).

See also Figure S4.

The ability to tightly regulate Raf-kinase activity in Schwann cells in the context of a normal nerve allows us to determine the role of this specific signaling pathway in Schwann cells in the broader inflammatory and regenerative response to injury. EM examination of the nerves from P0-RafTR animals following tamoxifen injection, revealed an increase in the size of the collagen-rich spaces between Schwann cell/axon units, which contained cells that were not present in control nerves (Figure 4A) and quantification confirmed this increase in cell number (Figure 4B). We also observed a large increase in p75-positive cells, presumably largely due to the dedifferentiation of myelinating cells to a progenitor-like state (Figure 4B). Moreover, proliferation markers showed there was considerably more proliferation in the nerves from injected P0-RafTR mice compared to controls and that a significant proportion of these proliferating cells were Schwann cells (Figures 4C and S4).

When peripheral nerves are injured, inflammatory cells are recruited to the injury site and throughout the distal stump where they aid in the clearance of myelin debris—a prerequisite for efficient nerve regeneration (Chen et al., 2007). Following a physical trauma, chemoattractants are released which attract inflammatory cells. Naked axons, myelin debris, and dedifferentiated Schwann cells have all been proposed as potential sources of such inflammatory signals (MacDonald et al., 2006; Martini et al., 2008). As aberrant inflammatory responses have been linked both to peripheral neuropathies and the development of peripheral nerve tumors, it is important to determine the cellular and molecular basis of these responses (Martini et al., 2008; Meyer zu Hörste et al., 2007; Parrinello and Lloyd, 2009; Staser et al., 2010). To address whether Raf/MEK/ERK signaling in Schwann cells is involved in the recruitment of inflammatory cells, we compared P0-RafTR nerves to control nerve sections using a panel of inflammatory cell markers (Figures 5 and S5). Remarkably, in nerves from injected P0-RafTR mice, we observed a large increase in the number of macrophages, mast cells, neutrophils, and T cells, all of which have been shown to be recruited into nerves following injury (Figures 5A–5E and S5A–S5C). These results were confirmed by analysis of EM sections, where large numbers of macrophages and mast cells could be seen (Figures 5A and S5C). However, one cell type, fibroblasts, which are found in large numbers in damaged nerves were not recruited into P0-RafTR nerves following tamoxifen injection (Figure S5D), suggesting that Schwann cells may not be responsible for recruiting fibroblasts to damaged nerves. Interestingly, the influx of inflammatory cells mirrored the response seen following an injury, with neutrophils entering the nerve at day 3, followed by macrophages, mast cells and T cells at around day 5 with the numbers increasing over time (Hall, 2005; Mueller et al., 2003). Importantly, at day 5, there was no observable myelin breakdown—suggesting that signals from dedifferentiated Schwann cells, rather than axons or myelin debris, are responsible for recruiting inflammatory cells.

The simplest explanation for our findings is that substances secreted by Raf-activated Schwann cells were directly responsible for the inflammatory response. We therefore tested whether

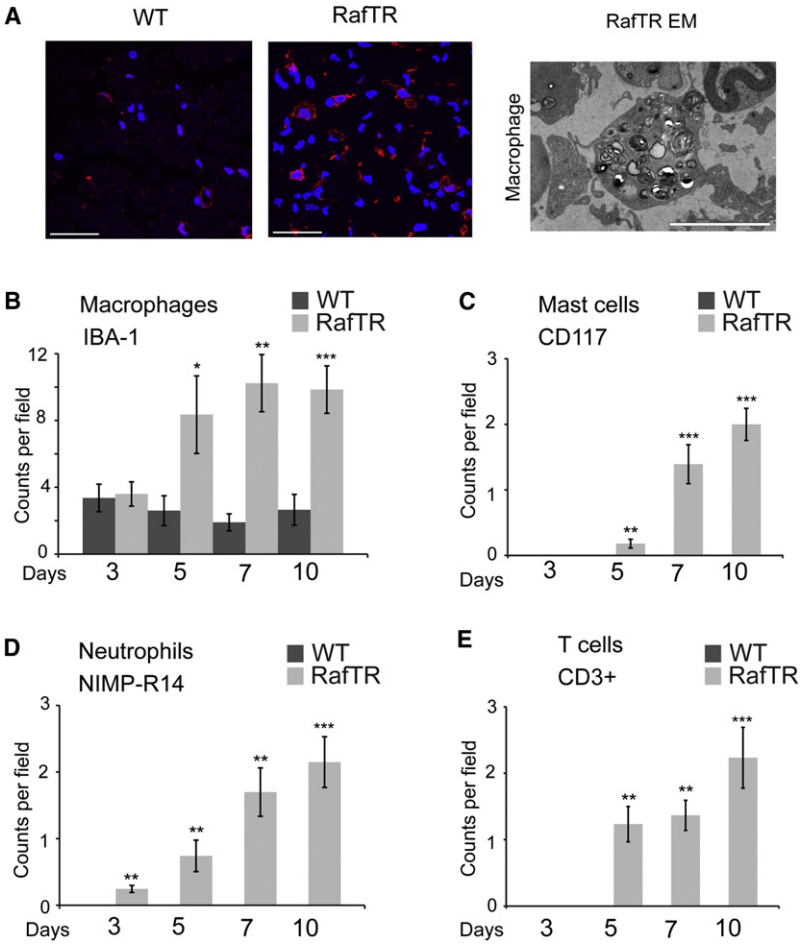

Figure 5. Inflammatory Cells Are Rapidly Recruited into Peripheral Nerves following Raf Activation in Schwann Cells

(A) Left panel: representative images of sciatic nerve cross-sections immunolabeled for the macrophage marker, Iba1 (red) and nuclei stained with Hoechst (blue). Scale bar is 25 μm. Right panel: an electron micrograph image showing a macrophage in the P0-RafTR sciatic nerve. Scale bar is 5 μm.

(B) Quantification of macrophage number as determined by Iba1/Hoechst staining of sciatic nerve cryosections for indicated time points in tamoxifen treated control WT and P0-RafTR mice.

(C–E) Similar quantification with antibodies specific to the (C) mast cell marker CD117; (D) neutrophil marker NIMP-R14 and (E) T cells marker CD3. (For all experiments: n = 3 animals for each group at each time point, 8 different fields for each animal were counted, data are represented as mean values ± SEM).

See also Figure S5.

conditioned medium (CM) from cultures of tamoxifen-treated rat Schwann cells expressing the RafTR (NSRafER) (Lloyd et al., 1997) was able to attract inflammatory cells in a similar fashion to that seen in vivo. We collected blood from adult rats, purified the white blood cell fraction and found that CM from tamoxifen-treated cells attracted significantly more monocytes, T cells, and granulocytes compared to vehicle-treated controls (Figures 6A and S6A). Moreover, this response was dependent on signaling through the ERK pathway confirming the specificity of the response. In contrast, CM from tamoxifen-treated cells was unable to attract more fibroblasts suggesting that cytokines produced by dedifferentiated Schwann cells do not promote fibroblast attraction which is consistent with the lack of a fibroblast response in the RafTR nerves (Figure 6A).

To determine the Schwann cell-derived molecules which may be involved in mediating the inflammatory response, we re-examined a microarray analysis performed on NSRafER cells (Parrinello et al., 2008) and found that a number of mRNAs encoding secreted factors were upregulated following Raf activation in dedifferentiated Schwann cells (Table 1). These included cytokines, some of which had been previously implicated in attracting inflammatory cells following nerve trauma such as the c-kit ligand and MCP-1 (Perrin et al., 2005; Toews et al., 1998; Tofaris et al., 2002) but also many others not previously reported in injured nerves—such as IL11, Scye1 and Cxcl10 (Table 1). Interestingly, a number of other factors likely to be important in the regenerative response, such as MEGF10—an engulfment receptor implicated in the phagocytosis of myelin debris (MacDonald et al., 2006), neuronal growth factors such as GDNF, and blood vessel growth factors (VEGFA and C) were also strongly upregulated. Importantly, the upregulation of many, but not all, of these genes in vivo was confirmed by qRT-PCR analysis (Figure 6B). Moreover, analysis of CM from NSRafER cells using a rat cytokine antibody array showed that the cytokines on the array, which were upregulated in the microarray analysis (MCP-1, VEGF, and TIMP-1), were also found at increased levels in the CM, confirming that the increase in mRNA is accompanied by a corresponding increase in cytokine production (Figure S6B). The majority of the cytokines on the antibody array, however, were not upregulated in the microarray analysis and we could not detect increased levels of these cytokines in the CM indicating a specificity of the response. The one exception was PDGF-AA, which was not upregulated in the microarray analysis but was found at slightly higher levels in the CM and in vivo. It will be of great interest to explore the role of these candidates in the regenerative process.

The PNS is a privileged environment maintained by the BNB. Breakdown of the BNB is thought to be required for the robust inflammatory response that occurs following nerve injury (Weerasuriya, 1988). To test the effects of activation of the ERK signaling pathway in Schwann cells on the BNB, we injected WT or P0-RafTR mice with Evans blue, a tracer that passes from blood vessels into the endoneurium and perineurium following breakdown of the BNB. In WT animals, the dye was restricted from the inner spaces of the sciatic nerve (Figure 6C). In contrast, in P0-RafTR animals, breakdown of the BNB was observed as early as day 4, with complete breakdown by day 5, coincident with the increased numbers of inflammatory cells found within

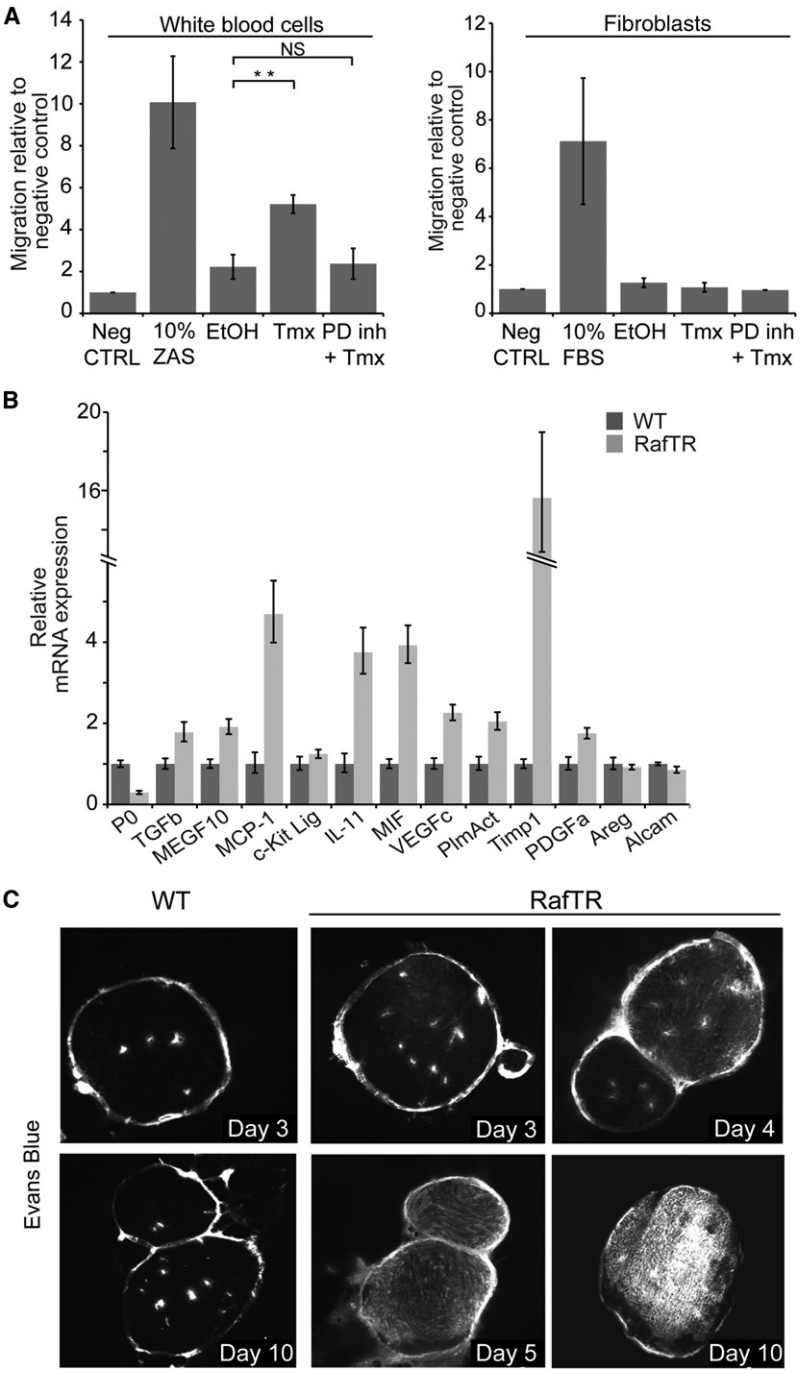

Figure 6. Dedifferentiated Schwann Cells Secrete Factors that Recruit Inflammatory Cells

(A) Conditioned medium from Schwann cells expressing the RafTR (NSRafER) pretreated for 48 hr with ethanol (EtOH), Tmx, Tmx plus the MEK inhibitor (PD184352), or control medium (Neg CTRL) was incubated in the bottom of duplicate transwells. Left panel: purified rat white blood cells were added to the upper wells. Two hours later, migrated cells were collected and counted by FACS. 10% Zymosan-activated serum (ZAS) was used as a positive control. Right panel: primary rat fibroblasts were added to the upper wells. 7 hr later, cells on the upper surface were removed mechanically and cells that had migrated into the lower surface were counted. 10% fetal bovine serum (FBS) was used as a positive control. Results are expressed as mean relative to control medium and are the average of 3 experiments ± SEM.

(B) qRT-PCR of RNA from sciatic nerves of WT and P0-RafTR mice after 72 hr of daily tamoxifen injections. The bar graphs represent the relative levels of indicated genes (n = 4 animals for each group, ± SEM).

(C) Evans blue dye was injected into WT and P0-RafTR mice 30 min before sacrifice at the indicated times following the first Tmx injection. Representative fluorescent images of sciatic nerve cross-sections from WT and P0-RafTR mice are shown (three animals at each time point were analyzed and all animals responded similarly).

See also Figure S6.

the nerve (Figures 5 and 6C). These results indicate that breakdown of the BNB can be triggered by Raf-activated signals from Schwann cells independent of trauma.

These findings show that that the activation of the ERK-signaling pathway in myelinating Schwann cells is sufficient to drive both demyelination and the inflammatory response with important implications for pathologies such as inflammatory neuropathies. To test the requirement of this pathway following injury, we used the highly-selective MEK1/2 inhibitor PD0325901 (Solit et al., 2006) to block the increase in ERK signaling seen in Schwann cells following nerve injury compared to the vehicle-treated controls. In initial experiments, we found that treatment of the mice reduced P-ERK levels dramatically as detected by both western blot and immunostaining (Figures S7A and S7B), although we were unable to block the pathway completely. In contrast, levels of P-JNK remained constant (Figure S7A). Despite this, we observed a dramatic inhibition of both Schwann cell dedifferentiation and the inflammatory response in the PD0325901 treated animals following nerve injury even though the axons degenerated similarly in the two conditions (Figure S7B). qRT-PCR analysis of the expression of the myelin genes *P0*, *periaxin*, and *MBP* showed there was a strong delay in the downregulation of these genes and a significant decrease in the level of inhibition in the PD0325901-treated animals (Figure 7A). Furthermore, we also saw a slight upregulation of some of these genes prior to injury consistent with the ERK pathway acting as a negative regulator of their expression. Moreover, there was a corresponding delay and inhibition of the upregulation of markers for the progenitor-like Schwann cells. Consistent with the inhibition of the transcriptional program associated with the switch in Schwann cell-state, we observed a dramatic difference in the structure of the nerves following injury (Figures 7B and S7C). Together, these results show that the ERK pathway is important in driving the rapid dedifferentiation of Schwann cells following

Table 1. Fold Increase in the RNA Levels of Selected Transcripts following Raf Activation in Schwann Cells

Gene Name		Fold Change	p Value
Neurite Outgrowth			
Alcam	Activated leukocyte cell adhesion molecule	12.31	1.31E-04
Boc_predicted	Biregional cell adhesion molecule-related, downregulated by oncogenes (Cdon), binding protein	2.96	3.46E-04
Gdnf	Glial cell derived neurotrophic factor	2.42	2.41E-03
Itga7	Integrin alpha 7	2.43	4.78E-03
Sema3a	Sema domain, immunoglobulin domain (Ig), short basic domain, secreted, (semaphorin) 3A	4.97	3.85E-04
Sgk	Serum/glucocorticoid-regulated kinase 1	3.10	2.04E-04
Phgdh	Similar to 3-phosphoglycerate dehydrogenase; phosphoglycerate dehydrogenase	2.42	2.99E-04
Slit3	Slit homolog 3 (*Drosophila*)	2.04	4.11E-03
Spon1	Spondin 1	16.93	8.03E-04
Angiogenesis			
Scg2	Secretogranin II (chromogranin C)	16.30	2.96E-04
Vegfa	Vascular endothelial growth factor A	2.13	9.82E-05
Vegfc	Vascular endothelial growth factor C	10.65	1.57E-05
SC Migration			
Cd44	Cd44 molecule	2.44	1.60E-04
Cdh2	Cadherin 2	3.36	7.13E-04
Cfl1	Cofilin 1, nonmuscle; similar to Cofilin-1 (cofilin, nonmuscle isoform)	1.94	1.95E-04
RGD1306694_predicted	Coiled-coil domain containing 88A	1.81	7.13E-04
Coro1a	Coronin, actin-binding protein 1A	2.72	7.65E-04
Gja1	Gap junction protein, alpha 1	65.95	2.23E-08
Itga3_predicted	Integrin alpha 3	4.28	1.78E-05
Kbtbd10	Kelch repeat and BTB (POZ) domain containing 10	3.04	1.67E-05
Msn	Moesin	1.97	5.44E-05
Podxl	Podocalyxin-like	1.96	9.69E-04
Ptprm	Protein tyrosine phosphatase, receptor type, M	3.45	1.35E-06
Scarb1	Scavenger receptor class B, member 1	2.27	4.79E-03
Tgfb1	Transforming growth factor, beta 1	4.41	1.59E-05
Tiam1_predicted	T-cell lymphoma invasion and metastasis 1 (predicted)	2.43	8.43E-06
Tnfrsf12a	Tumor necrosis factor receptor superfamily, member 12a	2.89	2.13E-05
Vasp_predicted	Vasodilator-stimulated phosphoprotein	1.92	5.44E-04
Cspg2	Versican	3.61	7.95E-04
SC Proliferation			
Calca	Calcitonin/calcitonin-related polypeptide, alpha	9.74	1.35E-05
Plau	Plasminogen activator, urokinase	3.11	1.72E-03
Unc5b	Unc-5 homolog B (C. elegans)	5.87	8.75E-07
Tgfb1	Transforming growth factor, beta 1	4.41	1.59E-05
Tissue Remodeling			
Dtr	Heparin-binding EGF-like growth factor	12.94	4.48E-05
Fgf2	Fibroblast growth factor 2	8.31	4.44E-07
Fbln1_predicted	Fibulin 1 (predicted)	4.32	6.68E-06
Hmox1	Heme oxygenase (decycling) 1	3.19	1.55E-05
Jag1	Jagged 1	7.43	5.24E-07
Mmp16	Matrix metalloproteinase 16	4.21	1.42E-03
Pthlh	Parathyroid hormone-like peptide	3.96	3.93E-04
Ptprm	Protein tyrosine phosphatase, receptor type, M	3.45	1.35E-06

Table 1. *Continued*

Gene Name		Fold Change	p Value
Sdc1	Syndecan 1	41.23	5.48E-08
Spp1	Secreted phosphoprotein 1	2.12	3.32E-04
Tnfrsf11b	Tumor necrosis factor receptor superfamily, member 11b (osteoprotegerin)	14.10	2.09E-06
Inflammation			
Areg	Amphiregulin	45.49	3.99E-07
Ccl2 (MCP1)	Chemokine (C-C motif) ligand 2	30.23	5.86E-07
Cxcl10	Chemokine (C-X-C motif) ligand 10	3.81	8.49E-07
Il11	Interleukin 11	4.86	3.04E-04
Kitl	Kit ligand	2.54	5.51E-03
Mif	Macrophage migration inhibitory factor	3.95	4.79E-06
Mmp14	Matrix metalloproteinase 14 (membrane-inserted)	1.80	6.85E-04
Megf10	Megf10 protein	14.55	2.08E-05
Plau	Plasminogen activator, urokinase	3.11	1.72E-03
Scye1	Small inducible cytokine subfamily E, member 1	1.71	6.41E-04

injury. Remarkably, we also observed a strong effect on the proliferative and inflammatory responses to nerve injury. For these experiments, we decided to perform a nerve crush rather than a transection and examined the nerves distal to the site of injury in order to minimize the inflammatory response directly caused by the trauma of the surgery. Analysis of the nerves showed that the MEK inhibitor blocked the increase in cell number seen following nerve injury and consistent with this, we observed a dramatic reduction of EdU-positive cells (Figures 7C, 7D, and S7D). Moreover, consistent with our in vitro studies (Figure 6A), there was a strong decrease in the number of inflammatory cells recruited into the nerve of PD0325901-treated mice compared to vehicle-treated controls (Figure 7E), consistent with the ERK pathway having an important role in the recruitment of inflammatory cells following nerve injury.

Continued observation of the P0-RafTR mice indicated that from day 10, the motor function of the mice progressively recovered and that by day 30 the mice performed as WT controls (Figure 8A and Movie S3). Analysis of the levels of ERK activation following the final injection on day 5 showed a strong decrease in P-ERK levels by day 10, with the levels back to control by day 14 (Figures S8A and S8B). Consistent with this, Schwann cell proliferation was also low by day 10 (Figure 4C). When the nerve histology was analyzed ''postrecovery'' on day 90, there was extensive remyelination (Figure 8B) and a dramatic reduction in p75 staining indicating a switch-back to the myelinated state (Figure 8C). Moreover, the numbers of inflammatory cells had largely returned to control levels (Figure 8D) and the BNB was restored (not shown). Nevertheless, the nerves were clearly distinct from control nerves (Figure 8B), in that many axons appeared to have thicker myelin sheaths and the ratio of axon diameter to myelin thickness showed greater heterogeneity than control nerves (Figure S8C). However, the recovered nerves were also clearly distinct from nerves that had regenerated following nerve transection, in which the number of axons per field was greatly increased, reflecting the axonal sprouting which takes place during axonal regrowth (Figure S8C); moreover, areas containing minifascicular structures were frequently observed—as by others (Bradley et al., 1998)—but were never seen in the recovered P0-RafTR nerves.

These results indicate that activation of ERK signaling in myelinating Schwann cells drives them back to a dedifferentiated state despite the presence of signals from intact axons. However, as soon as the ERK signal diminishes, these dedifferentiated Schwann cells are able to rapidly redifferentiate in response to axonal signals (Michailov et al., 2004; Sherman and Brophy, 2005; Taveggia et al., 2005). This would indicate that in the presence of axons, the period of dedifferentiation is solely controlled by the duration of the ERK signal. To test this, we added a second set of three daily tamoxifen injections, starting on day 14 to prolong the period of ERK activation and found that this resulted in a longer period of motor function loss (Figure 8A). Interestingly however, the mice recovered with similar kinetics indicating that Schwann cell dedifferentiation can be maintained by continual signaling through the ERK signaling pathway and that on the removal of the signal the Schwann cells are able to respond to the axonal signals and redifferentiate.

DISCUSSION

The repair of injured peripheral nerves involves the coordinated action of multiple cell types. The normal initiator of this injury response is a signal from damaged axons warning of their intention to degenerate. This rapid, currently unknown, signal is detected by Schwann cells and interpreted as an instruction to dedifferentiate to a progenitor-like cell. While the remarkable plasticity of the Schwann cell in response to nerve damage has been extensively reported, the signaling events that control the switch in cell state remain poorly understood. Moreover, the overall role of progenitor-like Schwann cells in the regeneration process remains unclear. In this study, we have developed a mouse model in which we can specifically activate the Raf/MEK/ERK signaling pathway in myelinating Schwann cells and show that activation of this single pathway is sufficient to initiate the dedifferentiation process and uncovering a central role for the Schwann cell in orchestrating the repair response.

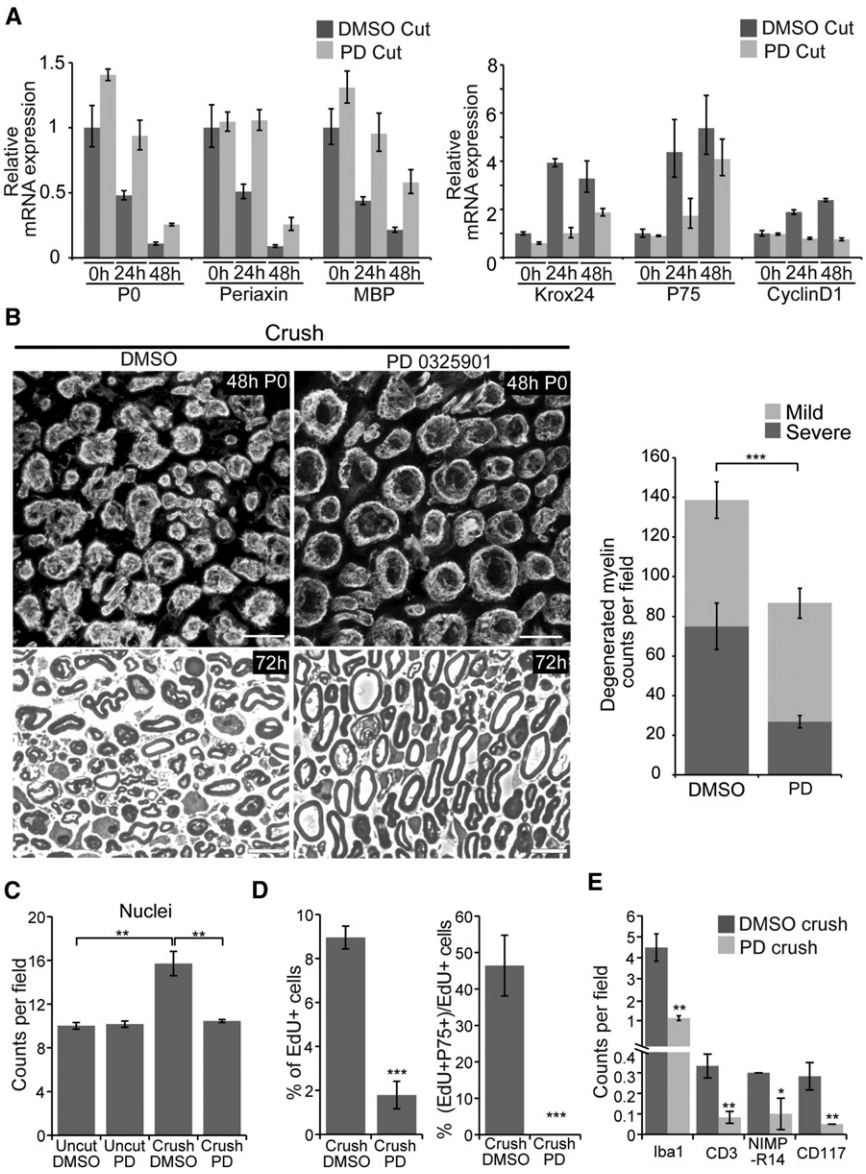

Figure 7. Inhibition of ERK Signaling Delays Schwann Cells Dedifferentiantion, Demyelination, and Induction of the Inflammatory Response that Follows Nerve Injury

(A) qRT-PCR of RNA from cut sciatic nerves of PD0325901 (PD cut)- or vehicle (DMSO cut)-treated mice. Three different time points are shown. The bar graphs represent the relative levels of indicated genes (n = 3 animals for each group ± SEM).

(B) Representative cross-sections of the distal regions of crushed sciatic nerves of PD0325901 (PD)- or vehicle (DMSO)-treated mice stained for P0 48 hr after crush (upper panels) or semi-thin cross-sections 72 hr after crush (lower panels). Scale bar 10 μm. Right panel: quantification of degenerated myelin fibers in PD or DMSO treated mice 72 hr after crush (n = 4 animals for each group, 3 different fields were counted for each animal, data are represented as mean values ± SEM). For details of Mild and Severe phenotypes, see Figure S7C.

(C) Cryosections of uninjured or crushed sciatic nerves of PD0325901 (PD)- or vehicle (DMSO)-treated mice were stained with Hoechst to label all the cells. Graph shows quantification of nuclei in the distal region of the nerves uninjured or 72 hr after crush.

(D) PD0325901 (PD)- or vehicle (DMSO)-treated mice were injected with EdU, 4 hr prior to sacrifice. Quantification of the percentage of EdU-positive cells and the percentage of EdU-positive cells that are P75 positive (proliferating Schwann cells) in the distal nerve 72 hr following crush.

(E) Quantification of macrophages (Iba1), T cells (CD3), neutrophils (NIMP-R14), and mast cells (CD117) in the distal region of crushed nerves from PD0325901 (PD)- or vehicle (DMSO)-treated mice at 72 hr. (For C–E, n = 3 animals for each group at each time point, 10 different fields for each animal were counted, data are represented as mean values ± SEM).

See also Figure S7.

Following nerve injury, Schwann cells respond to axonal damage with a strong, sustained activation of the ERK signaling pathway (Harrisingh et al., 2004). In the present study, we have overridden this sensing mechanism by activating this pathway in the absence of axonal damage. This drives the dedifferentiation process, demonstrating that sustained Raf/MEK/ERK signaling is sufficient to drive this switch in cell state and that it can act dominantly over any prodifferentiating signals provided by intact axons. This dominant control of cell state by Raf kinase is further demonstrated by the finding that prolonging ERK signaling maintains the dedifferentiated state, with the Schwann cells only responding to the prodifferentiating signals from axons once the level of ERK signaling declines. Importantly, the reversibility of these studies also showed that prodifferentiation signals are retained by axons in the adult, as the Schwann cells rapidly drop out of the cell cycle and redifferentiate once the ERK signal declines. Similarly to our in vitro results and consistent with other studies (Jessen and Mirsky, 2008), this change in cell state is reflected by a change in the transcriptional program of the Schwann cell. We find that this transcriptional response is relatively rapid, similar to that following injury and precedes any changes in the structure of the nerve, arguing that the transcriptional changes induced by Raf activation are driving the switch in cell state. This reprogramming of gene expression is followed by a slower breakdown of the myelin structure, presumably because of the relative stabilities of the proteins making up the myelin sheath, which may be enhanced by the integrity of the axons. Recent work has highlighted the role of the transcriptional regulators c-Jun and Notch (ICD) in the demyelination program initiated by nerve injury (Parkinson et al., 2008; Woodhoo et al., 2009). Interestingly, we find that *c-Jun* and the Notch ligand *jagged-1* are strongly upregulated following Raf activation in

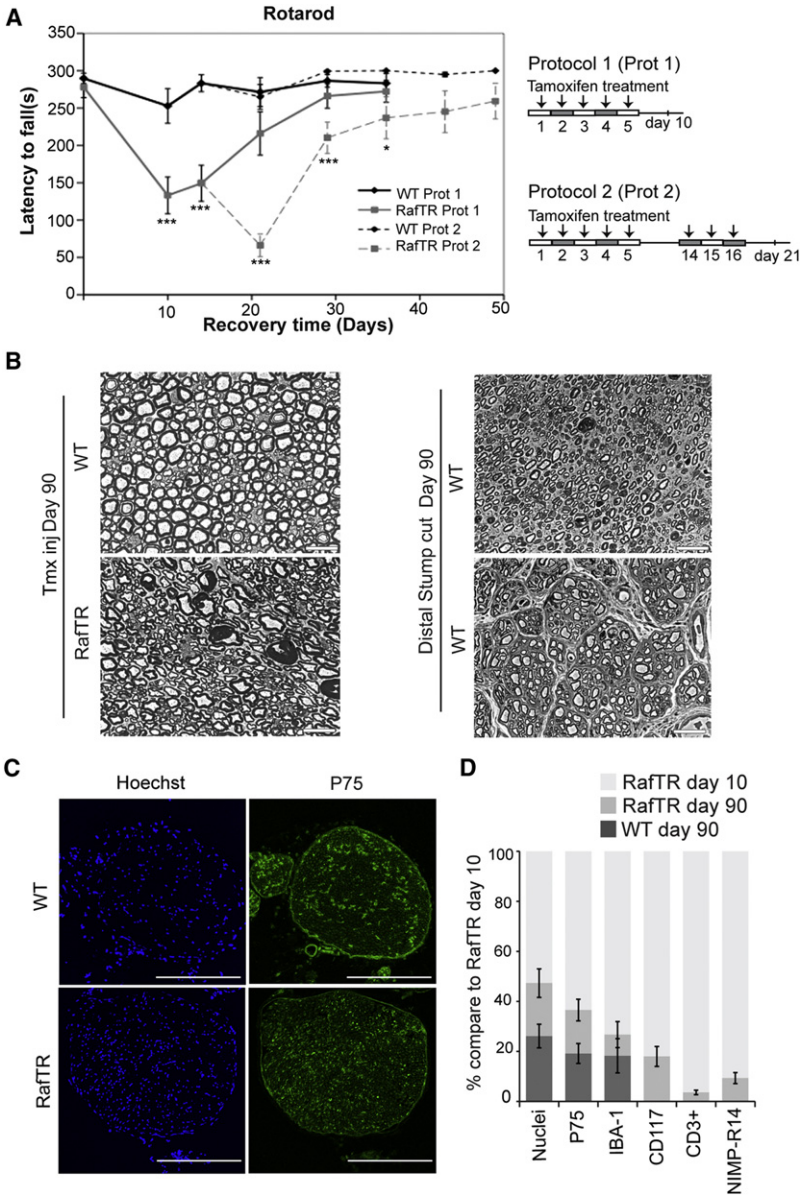

Figure 8. Remyelination and Behavioral Recovery of P0-RafTR Mice following the Cessation of Raf Signaling

(A) WT and P0-RafTR adult mice were tested on an accelerating rotarod for a maximum of 300 s at the indicated days using the two different tamoxifen injection protocols indicated. Mean latency to fall (±SEM) is plotted (n = 10 animals for each group).

(B) Representative phase microscopy images of semi-thin cross-sections of sciatic nerve stained with toluidine blue; Left panel: from WT and P0-RafTR mice 90 days after the first tamoxifen injection. Right panel: from the distal stump of "cut" WT nerve allowed to regenerate for 90 days. Scale bar is 20 μm.

(C) Cryosections of WT and P0-RafTR mice at day 90 stained with Hoechst (blue) and the Schwann cell marker p75 (green). Scale bar is 250 μm.

(D) Quantification of cell numbers from day 90 WT and recovered P0-RafTR nerves relative to day 10 values, expressed as a percentage. Data were obtained from analysis of cryosections labeled with Hoechst together with the antibodies to the indicated cell markers: p75 (dedifferentiated/nonmyelinating Schwann cells), Iba1 (macrophages), CD117 (mast cells), NIMP-R14 (neutrophils), and CD3 (T cells) (n = 3 animals for each group at each time point, 8 different fields from each animal were counted, data are represented as mean values ± SEM). See also Figure S8 and Movie S3.

Schwann cells (data not shown and Table 1), placing both c-Jun and the Notch pathway downstream of the ERK signaling pathway. It will be of great interest to further explore the relative roles of these and other transcription factors in this remarkable switch in cell state.

Part of the dedifferentiation response includes the induction of multiple genes that are potential mediators of the inflammatory response that follows activation of Raf in Schwann cells. In many aspects, this inflammatory response mirrors the response following nerve injury, indicating that Schwann cells are key mediators of this process—the influx of the inflammatory cells shows similar kinetics and the types of cells appear the same (Hall, 2005). This would seem to make biological sense—Schwann cells are early detectors of the damage signal, remain in the environment during the clearance and regeneration process, and redifferentiate to complete the repair and should thus be capable of initiating, maintaining, and limiting the inflammatory response. Our findings, that CM from Raf-activated Schwann cells is capable of attracting the white blood cells which we find in the nerve argues that this effect is direct. Some of these factors have been previously reported, such as MCP-1, which is thought to be important, although not the only factor responsible, for macrophage activation and recruitment (Fischer et al., 2008; Groh et al., 2010; Martini et al., 2008; Toews et al., 1998; Tofaris et al., 2002). In future studies, it will be important to investigate the roles of the other proteins identified in our studies on the inflammatory response.

It is interesting to speculate on the advantages of having Schwann cells coordinate this inflammatory response. The repair that occurs following peripheral nerve injury requires the coordination of multiple processes. At the site of injury, there is a classical wound-healing response, with the recruitment of inflammatory cells and fibroblasts, both of which are important in repairing the physical damage and defending the area from infection. However, the response to this wound has consequences far, sometimes more than a meter, from the initial site of injury and requires a distinct response, including the breakdown and clearance of axons downstream of the cut and the development of an environment suitable for regeneration. Although this response includes breakdown of the BNB and the influx of inflammatory cells, the major role of these cells is tissue remodeling rather than dealing with tissue trauma and

dangers of infection and is thus likely to require distinct signals and control mechanisms (Medzhitov, 2010). This view is corroborated by studies which have shown a distinct role for B cells in nerve regeneration—in that antibodies directed to myelin debris are crucial for the efficiency of the clearance process (Vargas et al., 2010). Our data show that Schwann cells instigate an inflammatory response via the secretion of a specific subset of cytokines. Analysis of this response compared to that elicited following trauma or infection may be useful to determine the different inflammatory responses to these distinct triggers.

Consistent with these ideas, an important distinction between the Raf-induced inflammatory response and the response following nerve trauma was the lack of a detectable fibroblast response. Following nerve crush or transection, large numbers of fibroblasts are found in the nerve. Moreover, as the nerve regenerates, fibroblasts are involved in tissue restructuring, forming compartmentalized units called minifascicles, which are thought to provide a protected microenvironment for the regrowing axons (Figure 8B; Morris et al., 1972). The lack of a detectable fibroblast response in the P0-RafTR nerves argues that Raf-mediated Schwann cell signals are not involved in controlling the behavior of these fibroblasts during the repair process. Consistent with this, we find that large numbers of fibroblasts tend to be restricted to the wound site (Parrinello et al., 2010), suggesting that signals associated with the damaged tissue are mediating this response. This also suggests that either trauma or axonal damage/regrowth is necessary for the formation of minifascicles, as these structures are never observed in the P0-RafTR mice.

Following nerve injury, in contrast to the P0-RafTR mouse, the axons degenerate and inflammation will occur as a direct response to the surgery and trauma. To determine the role of the MEK/ERK signaling pathway following injury, we treated mice with the MEK inhibitor and observed a dramatic inhibition in the kinetics in the switch in Schwann cell differentiation state and the inflammatory response. These results are consistent with our in vitro studies showing that MEK inhibitors are able to block Schwann cell dedifferentiation (Harrisingh et al., 2004) and the inflammatory response (Figure 6A). While these results indicate an important role for this pathway in both of these responses, we were unable to block the response completely. This may be due to our inability to completely block the pathway (we were unable to use higher concentrations of the inhibitor or treat for longer times due to toxicity in other tissues), a contribution of other pathways, or the loss of axonal prodifferentiating signals. However, they are consistent with an important role for this pathway both in the rapidity of the switch in Schwann cell state and the inflammatory response and moreover demonstrate the possibility of an approach for the treatment of disorders of the PNS, in particular inflammatory peripheral neuropathies. Future experiments using conditional knockouts of the ERK pathway should provide complementary information on the role of this pathway in the response and repair of peripheral nerves following injury.

Neurofibromas develop following loss of neurofibromin expression in Schwann cells. We have previously shown that *NF1* loss is sufficient to disrupt Schwann cell/axonal interactions in vitro as a result of elevated signaling through the Raf/MEK/ERK pathway and that this pathway blocks Schwann cell differentiation (Harrisingh et al., 2004; Parrinello et al., 2008). However, a recent flurry of in vivo studies in mice has demonstrated that Schwann cells engineered to lose NF1 expression during development differentiate normally (Joseph et al., 2008; Wu et al., 2008; Zheng et al., 2008). This suggested that either increased Raf/MEK/ERK signaling is unable to block Schwann cell differentiation in vivo or that during development this pathway does not get sufficiently activated in $NF1^{-/-}$ Schwann cells. Our results indicate the latter, as we show that Raf/MEK/ERK signaling is sufficient to both drive the efficient dedifferentiation of Schwann cells in normal nerve and that continual ERK signaling maintains them in this dedifferentiated state. It will be of great importance to determine the mechanisms by which ERK signaling is suppressed during development to allow myelination to proceed in NF1-deficient Schwann cells but can be triggered in adulthood to initiate neurofibroma development. Interestingly, a recent study has found that there is a requirement for ERK signaling at an early stage of Schwann cell differentiation during normal development (Newbern et al., 2011). Our results would suggest that the environment that permits $NF1^{-/-}$ cells to differentiate would also need to be acting during normal development to suppress this early signal. Another possibility is that it may indicate that different levels of ERK signaling have opposing effects on the differentiation process. This could be reminiscent of the dual role of neuregulin signaling in the control of Schwann cell myelination and demyelination (Syed et al., 2010). Consistent with this idea, P-ERK levels are extremely high and are maintained at this high level for several days in Schwann cells following nerve injury. The inducible, titratable nature of our mouse model may make it a useful system for studying further how differential activation of this pathway can affect Schwann cell differentiation state in vivo both during development and in the adult.

The results of this study also have potential significance for certain peripheral neuropathies, particularly those in which both demyelination and inflammation are observed. Elevated ERK signaling has been implicated in these disorders, making it likely that some aspects of the inflammatory response in these neuropathies are triggered by signals emanating from dedifferentiated Schwann cells (Kohl et al., 2010; Nadra et al., 2008; Tapinos et al., 2006). As these diseases progress, there tends to be increasing axonal damage (Nave, 2010). It is noteworthy that, at least in the short-term, there is no axonal damage associated with either the demyelination or the inflammatory response in the tamoxifen-injected P0-RafTR mouse. This is consistent with the view that Schwann cells provide trophic support to axons irrespective of their differentiation state (Nave, 2010) and that certain injuries can induce focal demyelination without associated axonal injury (Zochodne, 2008). However, it does suggest that the damage to axons seen in the disease states is either the result of a more prolonged response or requires additional factors. In any case, our findings that the Raf/MEK/ERK signaling pathway drives both the demyelination of peripheral nerves and the associated inflammatory response, together with the observations that recovery takes place when the signal is switched off indicate that inhibitors to this pathway or

downstream of this pathway may be useful therapeutics for the treatment of PNS neuropathies and tumors.

EXPERIMENTAL PROCEDURES

Generation of RafTR Transgenic Mice

The RafTR coding sequence was amplified by PCR from the vector pLXSN3-RAFTR using the forward 5′-CATTCCATGGAGTACTCACAGCCG-3′ and reverse primers 5′-CGATGACGTCAGATCGTGTTGGGGAAGC-3′, respectively. The resulting 2.2kb fragment was cloned directly into the AatII site of P0Cx32-Nco-Myc-Aat (A kind gift from Steven Scherer and John Bermingham, Jr.) following removal of the Myc-Tag ATG in the NcoI site. The vector backbone of P0Cx32-RafTR was removed using EcoRI/HindIII and the 7 kb fragment containing P0Cx32-RafTR was then used for pronuclear injection in C56BL6/J, which were then crossed and maintained on a B6CBAF1/J background. Genotyping of the RafTR transgene were performed using the primers (RafTR: 5′-GCAGCCCACACTGAGGATA-3′, 5′-AAGGACAAGGCAGGGCTATT-3′, hRaf1: 5′-ACCCATTCAGTTTCCAGTCG-3′, 5′-GCTACCAGCCTCTTCATTGC-3′). For details of tamoxifen injections and Evans blue injections, see Supplemental Experimental Procedures. All animal work was carried out in accordance with the guidelines and regulations of the Home Office.

Protein Analysis

For antibody, immunofluorescence and western blotting details see Supplemental Experimental Procedures.

Quantitative PCR

See Supplemental Experimental Procedures.

Microarray Analysis

The microarray analysis described previously in Parrinello et al. (2008) analyzed changes in RNA levels in NSRafER cells following 24 hr of Raf activation. Genes associated with distinct processes likely to be involved in nerve repair were identified using a combination of DAVID analysis (Huang et al., 2009) and manual identification. Relevant genes are expressed in Table 1. Fold change represents the level of induction following Raf activation compared to cells treated with control solvent and the associated p value is shown.

Cell Proliferation and Migration Analysis

See Supplemental Experimental Procedures.

Motor Coordination

Male mice (n = 10) were tested using the accelerating Rotarod. Rotarod speed was increased from 5 to 50 rpm over a 5 min period and the latency to fall was recorded. Twenty-four hours prior to each recording mice were subjected to 3 training trials, with a 20 min interval, in order to familiarize them with the procedure. During testing, three trials were recorded at each time point for each mouse.

Light and Electron Microscopy

Sciatic nerves were fixed with 2% glutaraldehyde in 0.2 M phosphate buffer O/N at 4°C, postfixed in osmium tetroxide for 1.5 hr at 4°C and then in 2% uranyl acetate for 45 min at 4°C. Nerves were then dehydrated in an ethanol series before embedding in epoxy resin. Semithin sections were cut with a glass knife at 0.3 μm and stained with 1% toluidine blue in 2% borax at 75°C for 2 min. Ultrathin sections were cut with a diamond knife at 70 nm, collected onto formvar coated slot grids and then visualized using transmission electron microscopy.

Statistical Analysis

The data are represented as mean values plus/minus standard error of the mean. Unpaired two-tailed Student's t test was used for statistical analysis and p values considered significant were indicated by asterisks as follows: *$p < 0.05$, **$p < 0.01$, ***$p < 0.001$.

SUPPLEMENTAL INFORMATION

Supplemental Information includes eight figures, three movies, and Supplemental Experimental Procedures and can be found with this article online at doi:10.1016/j.neuron.2011.11.031.

ACKNOWLEDGMENTS

This work was supported by a project grant from the AICR and by a programme grant from CRUK. A.W. was supported by a Programme Grant to K.R. Jessen and R. Mirsky from the Wellcome Trust. I.N. was partly supported by an EMBO fellowship. We would like to thank Steven Scherer and John Bermingham, Jr. for the P0 vector construct, the CRUK transgenic facility for the generation of the transgenic animals, UCL Biological Services for the maintenance of the animals and for useful advice, and Tomas Adejumo for help with the FACS analysis. We thank Martin Raff, David Parkinson, Rhona Mirsky, and Kristjan Jessen for critical reading of the manuscript.

Accepted: November 27, 2011
Published: February 22, 2012

REFERENCES

Bradley, J.L., Abernethy, D.A., King, R.H., Muddle, J.R., and Thomas, P.K. (1998). Neural architecture in transected rabbit sciatic nerve after prolonged nonreinnervation. J. Anat. *192*, 529–538.

Chen, Z.L., Yu, W.M., and Strickland, S. (2007). Peripheral regeneration. Annu. Rev. Neurosci. *30*, 209–233.

Choi, Y.K., and Kim, K.W. (2008). Blood-neural barrier: its diversity and coordinated cell-to-cell communication. BMB Reports *41*, 345–352.

Crawley, J.N. (2008). Behavioral phenotyping strategies for mutant mice. Neuron *57*, 809–818.

Fischer, S., Weishaupt, A., Troppmair, J., and Martini, R. (2008). Increase of MCP-1 (CCL2) in myelin mutant Schwann cells is mediated by MEK-ERK signaling pathway. Glia *56*, 836–843.

Groh, J., Heinl, K., Kohl, B., Wessig, C., Greeske, J., Fischer, S., and Martini, R. (2010). Attenuation of MCP-1/CCL2 expression ameliorates neuropathy in a mouse model for Charcot-Marie-Tooth 1X. Hum. Mol. Genet. *19*, 3530–3543.

Hall, S. (2005). The response to injury in the peripheral nervous system. J. Bone Joint Surg. Br. *87*, 1309–1319.

Harrisingh, M.C., Perez-Nadales, E., Parkinson, D.B., Malcolm, D.S., Mudge, A.W., and Lloyd, A.C. (2004). The Ras/Raf/ERK signalling pathway drives Schwann cell dedifferentiation. EMBO J. *23*, 3061–3071.

Huang, Y., Sirkowski, E.E., Stickney, J.T., and Scherer, S.S. (2005). Prenylation-defective human connexin32 mutants are normally localized and function equivalently to wild-type connexin32 in myelinating Schwann cells. J. Neurosci. *25*, 7111–7120.

Huang, W., Sherman, B.T., and Lempicki, R.A. (2009). Systematic and integrative analysis of large gene lists using DAVID bioinformatics resources. Nat. Protoc. *4*, 44–57.

Jessen, K.R., and Mirsky, R. (2008). Negative regulation of myelination: relevance for development, injury, and demyelinating disease. Glia *56*, 1552–1565.

Joseph, N.M., Mosher, J.T., Buchstaller, J., Snider, P., McKeever, P.E., Lim, M., Conway, S.J., Parada, L.F., Zhu, Y., and Morrison, S.J. (2008). The loss of Nf1 transiently promotes self-renewal but not tumorigenesis by neural crest stem cells. Cancer Cell *13*, 129–140.

Kohl, B., Fischer, S., Groh, J., Wessig, C., and Martini, R. (2010). MCP-1/CCL2 modifies axon properties in a PMP22-overexpressing mouse model for Charcot-Marie-tooth 1A neuropathy. Am. J. Pathol. *176*, 1390–1399.

Lloyd, A.C., Obermüller, F., Staddon, S., Barth, C.F., McMahon, M., and Land, H. (1997). Cooperating oncogenes converge to regulate cyclin/cdk complexes. Genes Dev. *11*, 663–677.

MacDonald, J.M., Beach, M.G., Porpiglia, E., Sheehan, A.E., Watts, R.J., and Freeman, M.R. (2006). The Drosophila cell corpse engulfment receptor Draper mediates glial clearance of severed axons. Neuron *50*, 869–881.

Martini, R., Fischer, S., López-Vales, R., and David, S. (2008). Interactions between Schwann cells and macrophages in injury and inherited demyelinating disease. Glia *56*, 1566–1577.

McClatchey, A.I. (2007). Neurofibromatosis. Annu. Rev. Pathol. *2*, 191–216.

Medzhitov, R. (2010). Inflammation 2010: new adventures of an old flame. Cell *140*, 771–776.

Meyer zu Hörste, G., Hartung, H.P., and Kieseier, B.C. (2007). From bench to bedside—experimental rationale for immune-specific therapies in the inflamed peripheral nerve. Nat. Clin. Pract. Neurol. *3*, 198–211.

Michailov, G.V., Sereda, M.W., Brinkmann, B.G., Fischer, T.M., Haug, B., Birchmeier, C., Role, L., Lai, C., Schwab, M.H., and Nave, K.A. (2004). Axonal neuregulin-1 regulates myelin sheath thickness. Science *304*, 700–703.

Morris, J.H., Hudson, A.R., and Weddell, G. (1972). A study of degeneration and regeneration in the divided rat sciatic nerve based on electron microscopy. IV. Changes in fascicular microtopography, perineurium and endoneurial fibroblasts. Z. Zellforsch. Mikrosk. Anat. *124*, 165–203.

Mueller, M., Leonhard, C., Wacker, K., Ringelstein, E.B., Okabe, M., Hickey, W.F., and Kiefer, R. (2003). Macrophage response to peripheral nerve injury: the quantitative contribution of resident and hematogenous macrophages. Lab. Invest. *83*, 175–185.

Nadra, K., de Preux Charles, A.S., Médard, J.J., Hendriks, W.T., Han, G.S., Grès, S., Carman, G.M., Saulnier-Blache, J.S., Verheijen, M.H., and Chrast, R. (2008). Phosphatidic acid mediates demyelination in Lpin1 mutant mice. Genes Dev. *22*, 1647–1661.

Nave, K.A. (2010). Myelination and the trophic support of long axons. Nat. Rev. Neurosci. *11*, 275–283.

Newbern, J.M., Li, X., Shoemaker, S.E., Zhou, J., Zhong, J., Wu, Y., Bonder, D., Hollenback, S., Coppola, G., Geschwind, D.H., et al. (2011). Specific functions for ERK/MAPK signaling during PNS development. Neuron *69*, 91–105.

Parkinson, D.B., Bhaskaran, A., Arthur-Farraj, P., Noon, L.A., Woodhoo, A., Lloyd, A.C., Feltri, M.L., Wrabetz, L., Behrens, A., Mirsky, R., and Jessen, K.R. (2008). c-Jun is a negative regulator of myelination. J. Cell Biol. *181*, 625–637.

Parrinello, S., and Lloyd, A.C. (2009). Neurofibroma development in NF1—insights into tumour initiation. Trends Cell Biol. *19*, 395–403.

Parrinello, S., Noon, L.A., Harrisingh, M.C., Digby, P.W., Rosenberg, L.H., Cremona, C.A., Echave, P., Flanagan, A.M., Parada, L.F., and Lloyd, A.C. (2008). NF1 loss disrupts Schwann cell-axonal interactions: a novel role for semaphorin 4F. Genes Dev. *22*, 3335–3348.

Parrinello, S., Napoli, I., Ribeiro, S., Digby, P.W., Fedorova, M., Parkinson, D.B., Doddrell, R.D., Nakayama, M., Adams, R.H., and Lloyd, A.C. (2010). EphB signaling directs peripheral nerve regeneration through Sox2-dependent Schwann cell sorting. Cell *143*, 145–155.

Perrin, F.E., Lacroix, S., Avilés-Trigueros, M., and David, S. (2005). Involvement of monocyte chemoattractant protein-1, macrophage inflammatory protein-1alpha and interleukin-1beta in Wallerian degeneration. Brain *128*, 854–866.

Samuels, M.L., Weber, M.J., Bishop, J.M., and McMahon, M. (1993). Conditional transformation of cells and rapid activation of the mitogen-activated protein kinase cascade by an estradiol-dependent human raf-1 protein kinase. Mol. Cell. Biol. *13*, 6241–6252.

Scherer, S.S., Xu, Y.T., Messing, A., Willecke, K., Fischbeck, K.H., and Jeng, L.J. (2005). Transgenic expression of human connexin32 in myelinating Schwann cells prevents demyelination in connexin32-null mice. J. Neurosci. *25*, 1550–1559.

Sherman, D.L., and Brophy, P.J. (2005). Mechanisms of axon ensheathment and myelin growth. Nat. Rev. Neurosci. *6*, 683–690.

Sheu, J.Y., Kulhanek, D.J., and Eckenstein, F.P. (2000). Differential patterns of ERK and STAT3 phosphorylation after sciatic nerve transection in the rat. Exp. Neurol. *166*, 392–402.

Solit, D.B., Garraway, L.A., Pratilas, C.A., Sawai, A., Getz, G., Basso, A., Ye, Q., Lobo, J.M., She, Y., Osman, I., et al. (2006). BRAF mutation predicts sensitivity to MEK inhibition. Nature *439*, 358–362.

Staser, K., Yang, F.C., and Clapp, D.W. (2010). Mast cells and the neurofibroma microenvironment. Blood *116*, 157–164.

Stoll, G., Jander, S., and Myers, R.R. (2002). Degeneration and regeneration of the peripheral nervous system: from Augustus Waller's observations to neuroinflammation. J. Peripher. Nerv. Syst. *7*, 13–27.

Suter, U., and Scherer, S.S. (2003). Disease mechanisms in inherited neuropathies. Nat. Rev. Neurosci. *4*, 714–726.

Syed, N., Reddy, K., Yang, D.P., Taveggia, C., Salzer, J.L., Maurel, P., and Kim, H.A. (2010). Soluble neuregulin-1 has bifunctional, concentration-dependent effects on Schwann cell myelination. J. Neurosci. *30*, 6122–6131.

Tapinos, N., Ohnishi, M., and Rambukkana, A. (2006). ErbB2 receptor tyrosine kinase signaling mediates early demyelination induced by leprosy bacilli. Nat. Med. *12*, 961–966.

Taveggia, C., Zanazzi, G., Petrylak, A., Yano, H., Rosenbluth, J., Einheber, S., Xu, X., Esper, R.M., Loeb, J.A., Shrager, P., et al. (2005). Neuregulin-1 type III determines the ensheathment fate of axons. Neuron *47*, 681–694.

Toews, A.D., Barrett, C., and Morell, P. (1998). Monocyte chemoattractant protein 1 is responsible for macrophage recruitment following injury to sciatic nerve. J. Neurosci. Res. *53*, 260–267.

Tofaris, G.K., Patterson, P.H., Jessen, K.R., and Mirsky, R. (2002). Denervated Schwann cells attract macrophages by secretion of leukemia inhibitory factor (LIF) and monocyte chemoattractant protein-1 in a process regulated by interleukin-6 and LIF. J. Neurosci. *22*, 6696–6703.

Vargas, M.E., Watanabe, J., Singh, S.J., Robinson, W.H., and Barres, B.A. (2010). Endogenous antibodies promote rapid myelin clearance and effective axon regeneration after nerve injury. Proc. Natl. Acad. Sci. USA *107*, 11993–11998.

Weerasuriya, A. (1988). Patterns of change in endoneurial capillary permeability and vascular space during Wallerian degeneration. Brain Res. *445*, 181–187.

Woodhoo, A., Alonso, M.B., Droggiti, A., Turmaine, M., D'Antonio, M., Parkinson, D.B., Wilton, D.K., Al-Shawi, R., Simons, P., Shen, J., et al. (2009). Notch controls embryonic Schwann cell differentiation, postnatal myelination and adult plasticity. Nat. Neurosci. *12*, 839–847.

Wu, J., Williams, J.P., Rizvi, T.A., Kordich, J.J., Witte, D., Meijer, D., Stemmer-Rachamimov, A.O., Cancelas, J.A., and Ratner, N. (2008). Plexiform and dermal neurofibromas and pigmentation are caused by Nf1 loss in desert hedgehog-expressing cells. Cancer Cell *13*, 105–116.

Zheng, H., Chang, L., Patel, N., Yang, J., Lowe, L., Burns, D.K., and Zhu, Y. (2008). Induction of abnormal proliferation by nonmyelinating schwann cells triggers neurofibroma formation. Cancer Cell *13*, 117–128.

Zochodne, D.W. (2008). Neurobiology of Peripheral Nerve Regeneration, First Edition (New York: Cambridge University Presss).